THE JOURNAL OF PHYSICAL CHEMISTRY C

Article

pubs.acs.org/JPCC

# Effect of Thermal Annealing in Ammonia on the Properties of InGaN Nanowires with Different Indium Concentrations

Christopher Hahn,[†] Amy A. Cordones,[†,‡] Sean C. Andrews,[†] Hanwei Gao,[†] Anthony Fu,[†] Stephen R. Leone,[†,‡,§] and Peidong Yang*[,†]

[†]Department of Chemistry, University of California, Berkeley, Berkeley, California 94720, United States, and Materials Sciences Division, Lawrence Berkeley National Laboratory, 1 Cyclotron Road, Berkeley, California 94720, United States

[‡]Chemical Sciences Division, Lawrence Berkeley National Laboratory, 1 Cyclotron Road, Berkeley, California 94720, United States

[§]Department of Physics, University of California, Berkeley, Berkeley, California 94720, United States

Supporting Information

**ABSTRACT:** The utility of an annealing procedure in ammonia ambient is investigated for improving the optical characteristics of $In_xGa_{1-x}N$ nanowires ($0.07 \leq x \leq 0.42$) grown on c-$Al_2O_3$ using a halide chemical vapor deposition method. Morphological studies using scanning electron microscopy confirm that the nanowire morphology is retained after annealing in ammonia at temperatures up to 800 °C. However, significant indium etching and composition inhomogeneities are observed for higher indium composition nanowires ($x$ = 0.28, 0.42), as measured by energy-dispersive X-ray spectroscopy and $Z$-contrast scanning transmission electron microscopy. Structural analyses, using X-ray diffraction and high-resolution transmission electron microscopy, indicate that this is a result of the greater thermal instability of higher indium composition nanowires. The effect of these structural changes on the optical quality of InGaN nanowires is examined using steady-state and time-resolved photoluminescence measurements. Annealing in ammonia enhances the integrated photoluminescence intensity of $In_xGa_{1-x}N$ nanowires by up to a factor of 4.11 ± 0.03 (for $x$ = 0.42) by increasing the rate of radiative recombination. Fitting of photoluminescence decay curves to a Kohlrausch stretched exponential indicates that this increase is directly related to a larger distribution of recombination rates from composition inhomogeneities caused by annealing. The results demonstrate the role of thermal instability on the improved optical properties of InGaN nanowires annealed in ammonia.

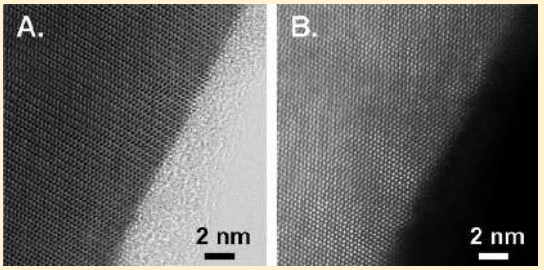


## INTRODUCTION

Over the past two decades, significant research has focused on the InGaN alloy due to its UV to IR band gap tunability, chemical stability, radiation resistance, and efficient emission properties. These collective properties make the InGaN ternary alloy an attractive candidate for applications such as color-tunable light-emitting diodes (LEDs), photovoltaics (PV), and photoelectrochemical (PEC) water splitting procedures.[1−5] However, the quantum efficiencies (QEs) for all types of processes in InGaN devices quickly drop off with increasing indium composition.[6] This decrease in device efficiency may be due to intrinsic strain-related factors such as a large thermodynamic miscibility gap and a lack of lattice-matched substrates.[2,7] These factors complicate the growth of single-crystalline, high indium composition InGaN with a low density of defects.

Recently, significant advancements have been made with the growth of single-crystalline higher indium composition InGaN using the strain-relieving properties of nanowire geometries.[8−11] In 2007, single-phase InGaN nanowires were grown within the bulk thermodynamic miscibility gap using a halide chemical vapor deposition (HCVD) method.[9] A unique property of HCVD-grown InGaN nanowires is the diminished effect of increasing indium composition on the InGaN photoluminescence (PL) efficiency. Modifications to the HCVD method have since enabled the epitaxial growth of homogeneous InGaN nanowire arrays on c-$Al_2O_3$ and c-GaN, which are free of the threading dislocations common in III-nitride thin films.[10] While threading dislocations can be avoided using the nanowire geometry, the poor QEs of early LED and PEC[3] devices fabricated using HCVD grown InGaN nanowires suggest that additional growth imperfections could play a role in the final device efficiency. These imperfections can include point defects, partial dislocations, and surface states that are known to introduce efficient nonradiative recombination pathways in InGaN.[2]

Annealing is a common post-treatment method for removing growth imperfections because it can supply the energy required for rearrangement of the lattice into a more thermodynamically stable configuration. Improved emission properties have been

Received: November 27, 2012
Revised: January 15, 2013

   dx.doi.org/10.1021/jp311685x | J. Phys. Chem. C XXXX, XXX, XXX−XXX

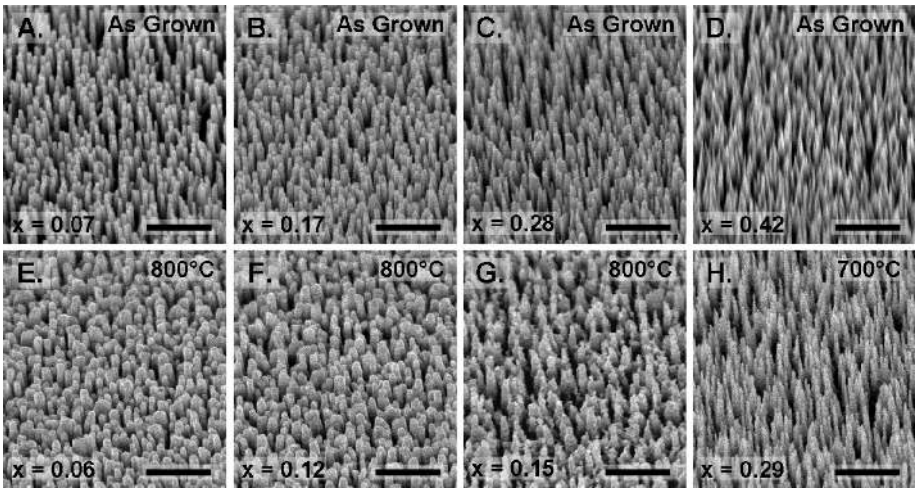


**Figure 1.** SEM images of as grown and annealed $In_xGa_{1-x}N$ nanowires. Tilted (45°) SEM images of as grown (A–D) and annealed (E–H) $In_xGa_{1-x}N$ nanowires on $Al_2O_3(001)$, demonstrating that samples retain the nanowire morphology after annealing. The image for each annealed nanowire array corresponds to the as grown sample directly above it. Compositions measured by SEM EDS show that the total indium content decreases after annealing (E–H), indicating that indium is preferentially etching from the lattice. Scale bar = 500 nm.

previously reported for InGaN thin films annealed in inert ($N_2$) and reactive gas atmospheres such as $NH_3$.[12,13] However, current difficulties with growing single-phase higher indium composition InGaN thin films have limited the studies on these stoichiometries. In addition, no such investigations exist on InGaN nanowires because of the newness of these materials. Here, we first use electron microscopy and diffraction techniques to examine the thermal and chemical stability of HCVD grown $In_xGa_{1-x}N$ nanowires ($0.07 \leq x \leq 0.42$) after a $NH_3$ annealing treatment. Structural changes are then correlated with the QEs and PL lifetimes to determine the effect of structural evolution on the photophysical properties of InGaN nanowires. It is shown that the thermal instability induced by a high-temperature annealing procedure can be used to improve the QE of InGaN nanowires by increasing the rate of radiative recombination.

## RESULTS AND DISCUSSION

**Morphology.** Single-phase $In_xGa_{1-x}N$ nanowires are epitaxially grown on $Al_2O_3(001)$ substrates for thermal annealing studies using a previously described halide chemical vapor deposition (HCVD) method.[10] Elemental analysis by scanning electron microscope (SEM) energy-dispersive X-ray spectroscopy (EDS) indicates nanowire array compositions of $x$ = 0.07, 0.17, 0.28, and 0.42 (Figure 1A–D). Samples are cleaved, and a section is subsequently annealed in an atmospheric pressure $NH_3$ environment (20 sccm flow) at 600, 700, or 800 °C for 1 h using a tube furnace and allowed to cool naturally.

Changes in morphology of the InGaN nanowire arrays are analyzed using SEM and scanning transmission electron microscopy (STEM) (Figure 1 and Figure SI1). The vertical orientation and heteroepitaxial growth of InGaN nanowires on $Al_2O_3(001)$ are confirmed using field-emission SEM images (Figure 1A–D). After annealing, all compositions are found to retain the nanowire morphology and orientation of the original array (Figure 1E–H). Although no significant change in length is observed, some increase in nanowire diameter occurs for arrays annealed at 800 °C (Figure 1E–G), indicating that the nanowires sinter at higher temperatures. In addition, high indium composition $In_xGa_{1-x}N$ nanowires ($x$ = 0.28, 0.42) exhibit surface roughening after annealing (Figure 1G,H). A closer examination of the morphologies using high-angle annular dark-field (HAADF) STEM confirms the trends of thermal instability and etching of higher indium composition nanowires (Figure SI1). Etch pits formed during the annealing have a triangular symmetry, indicating that there is some anisotropy to the etching of InGaN nanowires from $NH_3$ treatment. Similar roughening has been observed for III-nitride films annealed in $NH_3$ due to the formation of reactive hydrogen species at high temperature.[14]

**Composition.** Elemental analysis of annealed samples using EDS elucidates whether specific ions are being preferentially etched from InGaN nanowires. Reduced indium compositions are observed for each nanowire array after annealing, indicating that indium etches from the lattice during the post treatment procedure (Figure 1). A complete analysis of all annealing temperatures is shown in Table 1. The percent loss of indium is greater for nanowire samples with larger original indium compositions, which is consistent with the greater morphological changes observed for these samples. Therefore, the results indicate that indium is contributing to the thermal instability of InGaN nanowires in the high temperature $NH_3$ ambient.

**Table 1. EDS Compositions of Annealed $In_xGa_{1-x}N$ Nanowires**

| as grown | 600 °C | 700 °C | 800 °C |
|---|---|---|---|
| $x$ = 0.07 | 0.07 | 0.06 | 0.06 |
| $x$ = 0.17 | 0.17 | 0.14 | 0.12 |
| $x$ = 0.28 | 0.25 | 0.23 | 0.15 |
| $x$ = 0.42 | 0.38 | 0.29 | 0.17 |

Compositional fluctuations formed during annealing are characterized for individual nanowires using bright-field (BF) and HAADF high-resolution STEM (HRSTEM). Simultaneously captured BF and HAADF images of a nanowire from sample $x$ = 0.28 are shown in Figures 2A and 2B, respectively. A comparison of these images reveals no larger domains with $Z$-contrast, indicating that the as grown nanowire is homogeneous in composition on the nanometers scale. After annealing at 800


dx.doi.org/10.1021/jp311685x | J. Phys. Chem. C XXXX, XXX, XXX–XXX

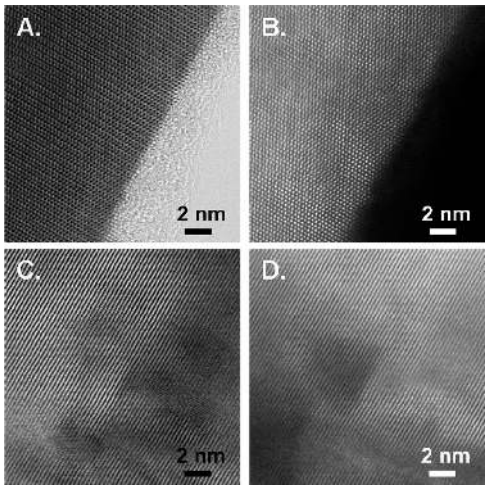


**Figure 2.** BF and HAADF HRSTEM images of as grown and annealed $In_xGa_{1-x}N$ nanowires. A comparison of (A) BF and (B) HAADF HRSTEM images from an $In_xGa_{1-x}N$ ($x$ = 0.28) nanowire shows that it is homogeneous in composition. After annealing at 800 °C, (C) BF and (D) HAADF HRSTEM images show triangular indium depleted regions, indicating that samples become inhomogeneous.

°C, surface roughening is responsible for most of the thickness contrast differences between simultaneously captured BF and HAADF images (Figure 2C,D). However, the HAADF image (Figure 2D) reveals an additional *Z*-contrast triangular region that is not observed in the BF image (Figure 2C). This darker area is gallium-rich, forming when indium is etched from the InGaN lattice.

**Structure.** The decomposition mechanism and thermal instability of InGaN nanowires are further analyzed using X-ray diffraction (XRD) (Figure 3). As grown arrays show predominantly the 002 wurtzite diffraction peak due to the aligned heteroepitaxial growth of $In_xGa_{1-x}N$ nanowires on $Al_2O_3$(001). Lower indium composition nanowires ($x$ = 0.07 and 0.17) show little change in their diffraction patterns after post-treatment (Figure 3A,B). A slight shift to larger diffraction angles is observed, further indicating the change in indium composition upon annealing. Compositional changes calculated from Vegard's law are consistent with those shown in Table 1. Thermal instability could also lead to phase separation, in the form of nanoscopic InGaN domains of different indium composition. However, the FWHM of the 002 peak remains unchanged after annealing for the $x$ = 0.07 and 0.17 samples (Figure 3A,B), and no additional peak formation is observed at higher diffraction angles after annealing at 800 °C for the $x$ = 0.17 sample (Figure SI2A). These results suggest that lower indium composition nanowires do not phase separate after annealing or that the composition fluctuations in these samples form on a subnanoscopic scale which is below our instrument resolution limit.

Nanowires with larger indium compositions ($x$ = 0.28 and 0.42) display more complex structural behavior when annealed at high temperatures (Figure 3C,D). Similar to lower indium composition arrays, a shift to larger diffraction angles is measured for samples annealed at or above 600 °C. However, an additional peak matching closely with the tetragonal 101 peak of indium metal can clearly be seen for arrays annealed at 800 °C. Lower intensity In 002 and 110 peaks are also observed for the $x$ = 0.42 sample (Figure SI2B). The formation of indium metal domains occurs from the decomposition of In−N bonds

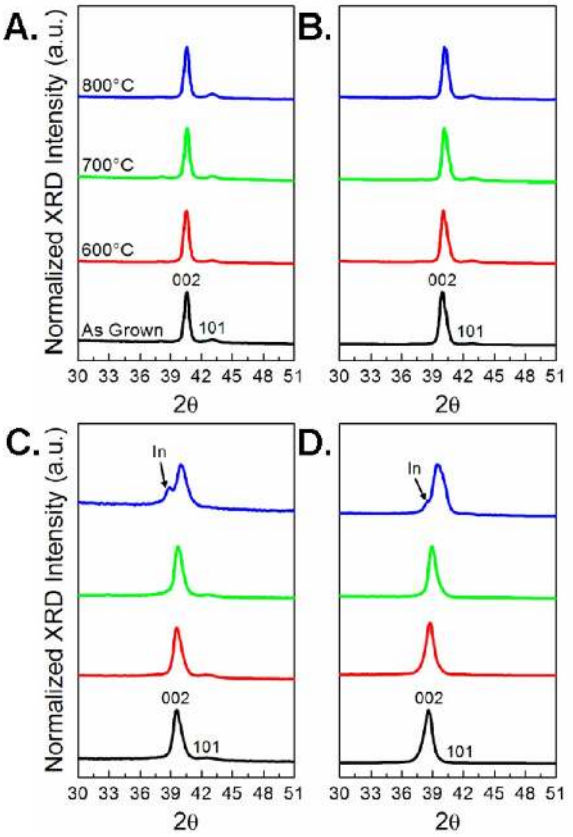


**Figure 3.** XRD spectra of as grown and annealed $In_xGa_{1-x}N$ nanowires. XRD spectra corresponding to samples (A) $x$ = 0.07, (B) $x$ = 0.17, (C) $x$ = 0.28, and (D) $x$ = 0.42 showing the wurtzite 002 and 101 peaks of $In_xGa_{1-x}N$ nanowires after annealing at a series of temperatures. Diffraction peaks shift toward higher angles because of a decrease in lattice constant from the etching of indium. Higher indium composition samples (C, D) show an additional In 101 peak from the decomposition of InGaN.

into indium metal and $N_2$ gas. Reactive hydrogen species formed from the decomposition of $NH_3$ are well-known to cause metal formation in III-nitrides at high temperature.[14] Indium metal can be further volatilized into the gas phase, therefore reducing the total indium composition. This decomposition mechanism is consistent with the morphology and composition changes observed for InGaN nanowires. Gallium metal formation was not observed because Ga−N bonds are much stronger than In−N bonds and are less likely to be broken at these temperatures.[15]

In addition to decomposition, the $x$ = 0.42 sample shows significant asymmetry of its wurtzite 002 peak (Figure 3D), indicating that $In_xGa_{1-x}N$ nanowires phase separate after annealing at 800 °C. Similar thermal instability is observed from annealing studies on single phase thin films of InGaN within the bulk thermodynamic miscibility gap.[7] At higher diffraction angles the indium tetragonal 103 peak and multiple wurtzite 103 peaks are observed in the annealed samples due to phase separation within InGaN nanowires (Figure SI2C). These results demonstrate the metastable nature of the high indium composition nanowires, which phase separate at higher temperatures. Furthermore, the observed thermodynamic instability bolsters the argument that higher indium composition single phase InGaN can only be grown using careful


dx.doi.org/10.1021/jp311685x | J. Phys. Chem. C XXXX, XXX, XXX−XXX

control of morphology (e.g., nanoscale geometry) and temperature.

While XRD was used to study the macroscopic structure of arrays, TEM was used to examine the structure of individual nanowires. High-resolution TEM (HRTEM) images show that InGaN nanowires are single crystalline as grown (Figure 4A–D). Low indium composition samples ($x$ = 0.07 and 0.17) remain single crystalline after annealing at 800 °C (Figure 4E,F); however, the higher composition samples display some polycrystallinity. The formation of grains near the surface for sample $x$ = 0.28 is shown in Figure 4G. This polycrystallinity could be a consequence of the volume reduction caused by the large amount of indium etched from the nanowires. Basal plane stacking faults are common in III-nitride materials and are observed for all of the as grown InGaN samples investigated here (Figure 4A–D). The prevalence of stacking faults can be attributed to their low formation energy in InN and GaN,[16] the poor surface mobility of adatoms at the low growth temperature used here,[17] and the fast reaction rates of HCVD. Investigation of annealed nanowires indicates that these stacking faults are not removed by this post-treatment. High-resolution TEM images show no major changes to the stacking faults (Figure 4E–H), even at high temperatures where the nanowires are unstable. A high pressure of $N_2$, typically used to suppress decomposition at very high temperatures, will not be effective since metastable InGaN nanowires are observed to phase separate. Therefore, the data suggest that removing stacking faults through post-treatment will be difficult due to the thermodynamic instability of InGaN nanowires.

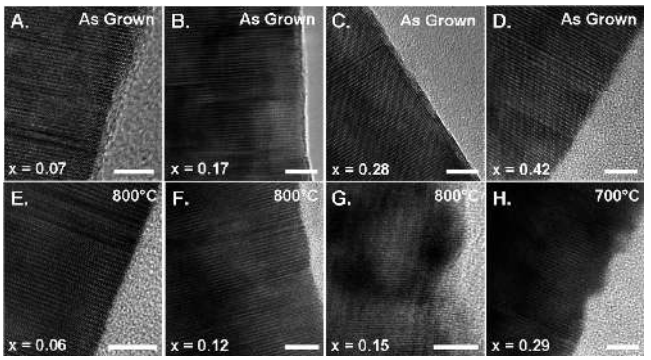


**Figure 4.** HRTEM images of as grown and annealed $In_xGa_{1-x}N$ nanowires. HRTEM images of individual nanowires from as grown samples (A) $x$ = 0.07, (B) $x$ = 0.17, (C) $x$ = 0.28, and (D) $x$ = 0.42 show that they are single crystalline. While the nanowires from sample (E) $x$ = 0.07 and (F) $x$ = 0.17 remain single crystalline after annealing at 800 °C, the nanowire from sample (G) $x$ = 0.28 becomes polycrystalline from the loss of indium. The crystallinity is maintained for sample (H) $x$ = 0.42 by reducing the annealing temperature. No change in the basal plane stacking fault density is observed after annealing. Scale bar = 5 nm.

In addition, HRTEM was used to determine the effects of sintering on the structure of InGaN nanowires. Merged nanowires are slightly shifted in lattice orientation as shown by the HRTEM image of nanowires ($x$ = 0.07) annealed at 800 °C (Figure SI3). This shift suggests a mosaic type of growth mode for InGaN nanowires on sapphire, which is common for III-nitride materials grown at low temperatures.[18,19] A high density of dislocations is observed at the interface of sintered nanowires that are twisted and/or tilted in orientation (Figure SI3). This increase in dislocation sites upon annealing likely results from the misalignment of the as grown arrays. These results indicate that sintering should be avoided to prevent new dislocations from forming during annealing.

**Steady-State and Time-Resolved Photoluminescence.** Photoluminescence measurements are used to examine the influence of annealing on the band-edge optical properties of InGaN nanowire arrays. Samples are excited with a 325 nm continuous-wave HeCd laser focused down to a spot size of 50 × 100 $\mu$m. PL spectra are collected on a single spot for each nanowire array using the same incident power, acquisition times, and microscope collection geometry. Further details can be found within the Experimental Section. Nanowire arrays of composition $x$ = 0.07 and $x$ = 0.17 (Figure SI4 and Figure 5A) show little change in peak wavelength and shape after annealing. This is in agreement with our structural analysis, which indicates that these compositions are still single phase after annealing. In contrast, the peak wavelength is found to blue-shift by 23 and 56 nm upon annealing at 800 °C for samples $x$ = 0.28 and 0.42, respectively (Figure 5B,C). This is consistent with the compositional changes observed for these samples because GaN has a larger band gap than InN. Furthermore, annealing the largest indium composition sample ($x$ = 0.42) at 800 °C leads to new peak shoulders below 400 nm and above 800 nm (Figure 5C). Structural characterization indicates sample $x$ = 0.42 phase separates at 800 °C. Therefore, the additional PL peaks for this sample are indicative of different composition domains that create new emission centers

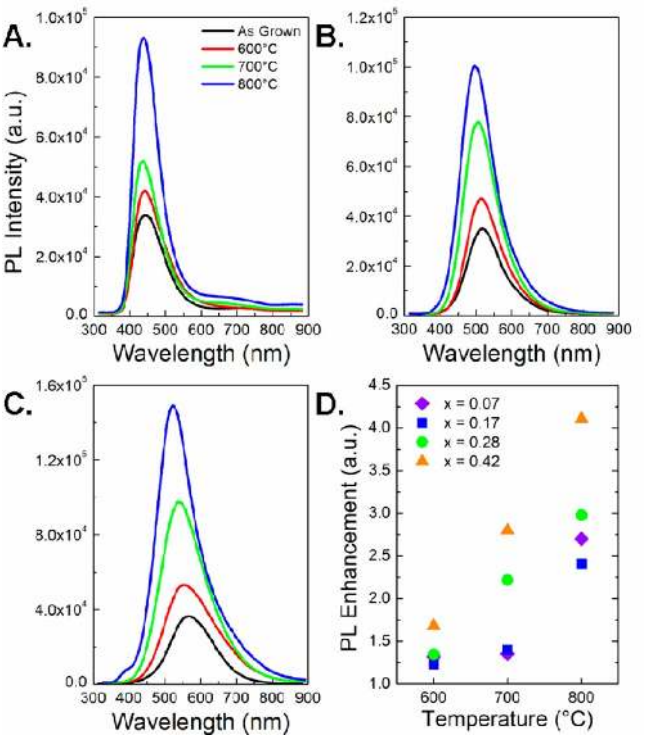


**Figure 5.** PL spectra of as grown and annealed $In_xGa_{1-x}N$ samples (A) $x$ = 0.17, (B) $x$ = 0.28, and (C) $x$ = 0.42 excited using a 325 nm HeCd laser. All compositions show an enhancement in emission with annealing temperature. The peak wavelength blue-shifts because of a reduction in band gap from the removal of indium. Additional peaks are formed for sample (C) $x$ = 0.42 from phase separation. (D) Integrated PL intensities show greater enhancements in QE for higher indium composition nanowire arrays.


dx.doi.org/10.1021/jp311685x | J. Phys. Chem. C XXXX, XXX, XXX–XXX

in InGaN. Color images of the emission from nanowire arrays are shown in Figure SI5. The results suggest that the annealing procedure could be tuned with higher indium composition arrays to obtain the desired broadening to obtain white light emission.

Photoluminescence spectra were further analyzed to determine the effect of indium composition and annealing on the QE of InGaN nanowires:

$$\mathrm{QE} = \frac{\text{photons out}}{\text{photons in}} \tag{1}$$

where "photons in" are the number of photons absorbed and "photons out" are the number of photons emitted. We first examined changes in QE using a previously described integrating sphere setup.[20] However, due to the low QE of InGaN nanowires, only an upper bound of <0.01% was obtained using this method. Instead, we integrate the PL intensities of spectra shown in Figure 5 to examine any changes in the "photons out". The "photons out" increases both with indium composition and annealing (Table 2). To determine

**Table 2. Integrated PL Intensities and Absorption Percentages of As Grown and Annealed $In_xGa_{1-x}N$ Nanowires**[a]

| | as grown | | annealed 800 °C | |
|---|---|---|---|---|
| $x$ | integrated PL intensity (au) | absorption (%) of 325 nm | integrated PL intensity (au) | absorption (%) of 325 nm |
| 0.07 | $1.439 \times 10^6$ | 96.4 | $3.886 \times 10^6$ | 97.2 |
| 0.17 | $3.589 \times 10^6$ | 99.3 | $8.648 \times 10^6$ | 98.5 |
| 0.31 | $4.374 \times 10^6$ | 99.4 | $1.302 \times 10^7$ | 98.5 |
| 0.44 | $5.638 \times 10^6$ | 99.5 | $2.316 \times 10^7$ | 98.0 |

[a]The uncertainties for integrated PL intensities are 0.5% and for absorption are 0.8%.

whether the increases in "photons out" correspond to changes in the QE, differences in "photons in" are also compared from the integrating sphere measurements. No significant changes in absorption percent of the incident 325 nm laser source are observed (Table 2), and therefore the QE increases with both increasing indium composition and annealing in $NH_3$. A PL enhancement factor is calculated by integrating the peaks of the annealed and as grown samples. This analysis (Figure 5D) indicates that the PL enhancement in lower indium composition nanowires ($x$ = 0.07, 0.17) requires a greater annealing temperature than for higher indium composition nanowires ($x$ = 0.28, 0.42). Therefore, the $x$ = 0.28 and 0.42 samples have the highest enhancement factors of 2.98 ± 0.02 and 4.11 ± 0.03, respectively, when annealed at 800 °C. By comparing these results to our structural characterization, there is a correlation between nanowire instability and an increase in QE.

To determine why the QE is changing, the excited state kinetics of InGaN nanowires is investigated by measuring the time-resolved PL. The resulting PL decay curves of as grown samples $x$ = 0.07, 0.17, 0.28, and 0.42 show a decrease in the excited state lifetime with increasing indium composition (Figure 6). Decay curves for the higher indium composition samples ($x$ = 0.28 and 0.42) approach the instrument response limit at shorter time durations, indicating that excited carriers could be recombining even faster than the instrumental response time.

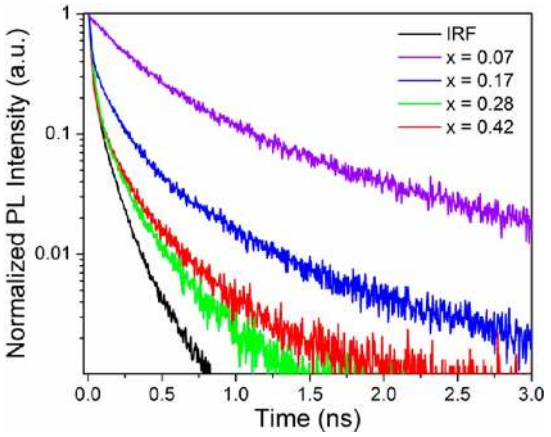


**Figure 6.** Time-resolved PL spectra of as grown $In_xGa_{1-x}N$ nanowires. Time-resolved PL spectra from samples excited using a 267 nm femtosecond pulsed laser show a decrease in PL lifetime with increasing indium composition. The fast initial decay of samples $x$ = 0.28 and 0.42 are limited by the instrument response function (IRF) plotted in black.

The excited state lifetime ($\tau$) for a single exponential decay can be expressed by the following equation:

$$\tau = \frac{1}{k_r + k_{nr}} \tag{2}$$

where $k_r$ and $k_{nr}$ correspond to the radiative and nonradiative decay rates, respectively. The observed decrease in $\tau$ could be due to an increase in either or both parameters. Furthermore, the excited state lifetime is related to the QE by the equation

$$\mathrm{QE} = \frac{\tau}{\tau_r} = \frac{k_r}{k_r + k_{nr}} \tag{3}$$

where $\tau_r$ represents the radiative lifetime. The PL intensities (325 nm excitation) and PL decays (267 nm excitation) can be compared here because no intrinsic excitation wavelength dependence of the QE has been observed for pristine nanoscale materials due to ultrafast intraband charge relaxation.[21] Organic surface ligands, which have been postulated to contribute to a wavelength dependence, are not expected to be on the surface since our InGaN nanowires are grown using a gas phase synthesis. Furthermore, the trends in PL intensity before and after annealing at 800 °C are consistent for both 267 nm (time-resolved PL) and 325 nm (steady-state PL) excitation. Using the boundary condition of QE < 0.01% determined by integrating sphere measurements, it is clear that $k_{nr} \gg k_r$, and eq 2 can be approximated as $\tau \approx 1/k_{nr}$. This QE boundary condition is true for all indium compositions, both as grown and annealed, and this condition is used throughout the remaining discussion. Using this approximation, the decrease in $\tau$ with increasing indium composition (Figure 6) indicates an increase in $k_{nr}$. This is consistent with previous reports for InGaN films, which indicate an increase in nonradiative recombination pathways with the incorporation of more indium.[2] Additionally, the QE was found to increase with indium composition (Table 2). Taken together, increases in both $\tau$ and QE with indium composition indicate that $k_r$ must also increase, and by a larger factor than $k_{nr}$.

The nonlinear shapes of the PL decays on a logarithmic scale indicate distributed/multiexponential kinetics for InGaN nanowires (Figure 6). These deviations from single-exponential


dx.doi.org/10.1021/jp311685x | J. Phys. Chem. C XXXX, XXX, XXX−XXX

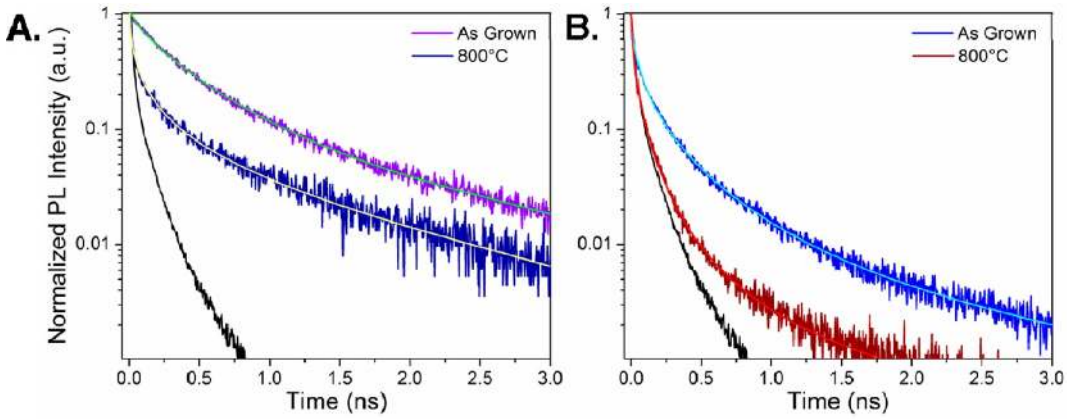


**Figure 7.** Time-resolved PL spectra of annealed $In_xGa_{1-x}N$ nanowires. Time-resolved PL spectra for samples (A) $x = 0.07$ and (B) $x = 0.17$ show a decrease in PL lifetime after annealing in ammonia. The stretched exponential fits are overlaid with each decay curve. Instrument response functions (IRF) are plotted in black.

behavior are common in InGaN systems because of disorder in the material.[8,22,23] The decay curves are fit to a Kohlrausch stretched exponential, modified to account for the substrate signal measured from bare c-$Al_2O_3$:

$$F \propto e^{-(t/\tau_k)^{\beta}} + I_{substrate}(t) \quad (4)$$

where $\tau_k$ is a characteristic lifetime and $\beta$ is the stretching parameter ranging from $0 < \beta \leq 1$.[24] When $\beta = 1$, the function simplifies to a single-exponential decay. A decrease in $\beta$ indicates a wider distribution of decay rates.[25] The substrate signal, $I_{substrate}(t)$, is measured independently and fit to a biexponential decay. The substrate signal decay times and ratio of preexponential factors are fixed while fitting the nanowire PL decay curves to eq 4. The average decay lifetime $\tau_a$ can be calculated from the stretched exponential according to the equation

$$\tau_a = \frac{\tau_k}{\beta}\Gamma\left(\frac{1}{\beta}\right) \quad (5)$$

where $\Gamma(n)$ is the gamma function.[25] The fits for the $x = 0.07$ and 0.17 samples can be seen in Figure 7, and the values of $\tau_k$, $\beta$, and $\tau_a$ are reported in Table 3. The $x = 0.28$ and 0.42 samples were not analyzed due to the previously mentioned uncertainty during the short time domain, but we note that they follow the same qualitative trends as the lower indium composition nanowires. Overall, decreases in both $\beta$ and $\tau_a$ are observed with increasing indium composition. The decrease in the $\beta$ parameter from 0.72 ± 0.03 to 0.45 ± 0.02 for the $x = 0.07$ and 0.17 samples, respectively, is attributed to an increase in atomic-scale indium fluctuations from alloy broadening, as explained below. The resulting energy fluctuations in the conduction and valence band of the alloy can reduce $\beta$ by forming a distribution of localized potential wells rather than extended states.[26] The excited carriers can become highly localized in these potential wells, thus increasing $k_r$ due to stronger overlap of the electron and hole.[27] Using eqs 2 and 3 to correlate $\tau_a$ and QE, both $k_{nr}$ and $k_r$ increase with indium composition by factors of 4.80 ± 0.05 and 11.6 ± 0.2, respectively.

**Table 3. Calculated Fitting Parameters for As Grown and Annealed $In_xGa_{1-x}N$ Nanowires**

| sample | $\tau_k$ (ns) | $\beta$ | $\tau_a$ (ns) |
|---|---|---|---|
| $x = 0.07$ as grown | 0.228 ± 0.015 | 0.719 ± 0.031 | 0.317 ± 0.024 |
| $x = 0.17$ as grown | 0.030 ± 0.006 | 0.452 ± 0.024 | 0.066 ± 0.015 |
| $x = 0.07$ annealed | 0.029 ± 0.010 | 0.465 ± 0.060 | 0.061 ± 0.027 |
| $x = 0.17$ annealed | 0.010 ± 0.004 | 0.438 ± 0.034 | 0.023 ± 0.010[a] |

[a]This sample's PL signal decays within the instrument response. The actual decay time may be faster than indicated by $\tau_a$ but was unresolved by this method.

The PL decay curves are also compared to quantitatively examine the effect of annealing in $NH_3$ at 800 °C. For all samples, the excited-state lifetime decreases (Figure 7 and Figure SI6) and the QE increases (Figure 5D and Table 2) after post-treatment at 800 °C. Here, only the $x = 0.07$ sample is considered quantitatively (Figure 7A) because the decay kinetics could no longer be resolved for the $x = 0.17$ sample after annealing (Figure 7B). The $\beta$ parameter decreases from 0.72 ± 0.03 to 0.47 ± 0.06 for the $x = 0.07$ sample, indicating that annealing increases the distribution of decay rates in InGaN nanowires (Table 3). Although no macroscopic structural changes are observed for this sample, the increase in distribution of rates suggests that additional recombination sites are formed during annealing. This could result from atomic rearrangement into indium rich regions during the high-temperature annealing of InGaN.[12] A decrease in the average excited state decay time was also observed upon annealing due to increases in both $k_{nr}$ and $k_r$. $\tau_a$ decreases from 0.32 ± 0.02 to 0.06 ± 0.03 ns (Table 3), indicating that $k_{nr}$ increases by a factor of 5.33 ± 0.09. It is possible to relate the change in $k_{nr}$ to the TEM results (Figure SI3), which show an increase in the density of dislocations in InGaN nanowires after annealing due to sintering. These dislocations can act as additional non-radiative recombination sites and therefore increase $k_{nr}$.[2] Taken together, the increase in QE (by a factor of 2.68 ± 0.04) and decrease in $\tau_a$ (by a factor of 5.33 ± 0.09) for the $x = 0.07$ sample indicate that the average $k_r$ increases by a factor of 14.3 ± 0.3 after annealing at 800 °C. Similar to our conclusion for as grown nanowires, it is suggested that this increase in $k_r$ is related to the composition fluctuations formed during annealing.

The observation that annealing can successfully improve the QE of InGaN nanowires suggests that such treatment may be useful for fluorescence-based applications. The PL lifetime studies indicate that the main mechanism for improving the QE


dx.doi.org/10.1021/jp311685x | J. Phys. Chem. C XXXX, XXX, XXX−XXX

is an increase in the radiative decay rate. Therefore, annealing could be useful for devices that require fast radiative recombination, such as LEDs. Furthermore, emission broadening is observed for higher indium composition arrays, which suggests that annealing could be used to control spectral features for white light emitters. These studies do show an increase in nonradiative recombination rates for annealed InGaN nanowires due to dislocations formed during sintering. However, it is proposed that additional control over the density of the as grown arrays by patterning the substrate could prevent this. Because annealing improves the QE by increasing the rate of radiative carrier recombination, it is unlikely that such a treatment would be useful for applications that require longer carrier lifetimes and diffusion lengths for charge collection, such as PV and PEC water splitting. For these applications, it will be necessary to increase the carrier lifetimes.[28] One issue affecting carrier lifetimes is surface recombination from a high density of surface states in InGaN nanowires. These defects can provide fast nonradiative decay pathways in the current samples. Surface passivation using materials that require low deposition temperatures such as AlN, $SiN_x$, $SiO_2$, and S could help to mitigate this issue.[29−31] Other issues include nonradiative recombination at point defects and partial dislocations, which are incorporated during the HCVD growth process. The structural studies show that the thermal instability of InGaN nanowires prevents the use of temperatures high enough to remove partial dislocations. Therefore, better results could be achieved by preventing the incorporation of such imperfections during growth. Investigations into the growth mechanism of III-nitrides have suggested that careful control of the III−V precursor ratio can prevent point defect and partial dislocation formation during growth.[32]

## CONCLUSIONS

In conclusion, we have examined changes in the structural, compositional, and optical properties of InGaN nanowires after thermal annealing in $NH_3$. Samples retained the nanowire morphology, although some thermal instability was observed from sintering and surface roughening at higher temperatures. This instability was confirmed through elemental analysis, which revealed that the total indium composition of InGaN nanowires was reduced due to etching from the lattice. Structural investigations of this instability showed that nanowires retained their crystallinity, but higher indium composition nanowires can decompose into indium metal because In−N bonds are weaker than Ga−N bonds. In addition, phase separation into different stoichiometries of $In_xGa_{1-x}N$ was observed in sample $x = 0.42$, indicating that higher composition InGaN nanowires are metastable. Optical studies revealed that this annealing procedure successfully increases the QE of InGaN nanowires and both the radiative and nonradiative carrier recombination rates. Furthermore, the annealed nanowires displayed more highly distributed decay kinetics, which we attribute to the observed composition inhomogeneities formed in InGaN nanowires during annealing. We propose such a treatment could be utilized to increase the radiative recombination rate in devices such as LEDs. Further work will be done to improve the QE by reducing the nonradiative recombination pathways for applications such as PV and PEC water splitting. For this, we suggest growth modifications as well as post treatment methods such as surface passivation.

## EXPERIMENTAL SECTION

SEM images and correlated EDS spectra were taken using a JEOL JSM-6340F field emission scanning electron microscope equipped with an EDAX Falcon detector. EDS data were collected from the Ga K and the In L peaks of a 40 $\mu$m × 40 $\mu$m area for each sample at 20 kV and analyzed using the software's true standardless-quantification mode.

XRD patterns were taken using a Bruker AXS D8 Advance diffractometer, which used an incident Co K$\alpha$ radiation of 1.790 26 Å. Spectra were collected by fixing samples onto a flat puck.

HRTEM images were taken using a JEOL JEM-2100 LaB6 microscope at 200 kV. STEM images were obtained in both an FEI Tecnai F20-UT and FEI Titan 3 80-300 operated at 200 and 300 kV, respectively. The Titan is equipped with two CEOS hexapole-type spherical aberration correctors, allowing for subangstrom resolution. HAADF images were acquired at a collection angle of ∼110 mrad. Both BF and HAADF images were acquired simultaneously.

For steady-state PL measurements, nanowire arrays were excited by a 325 nm continuous-wave (CW) HeCd laser with a 5 mW unpolarized beam focused to a spot size of 50 × 100 $\mu$m. PL spectra were collected on a single spot for each sample with a 1 s exposure time and accumulated 10 times through a 50× objective on a Nikon microscope. Signals were routed to a liquid $N_2$ (LN) cooled CCD/spectrometer (PI Acton) via an optical fiber. Instrumental uncertainty for steady-state PL measurements was measured to be 0.54%.

Absorption percentages were measured using a custom 4 in. diameter integrating sphere (Gigahertz Optik UPK-100-L coated with ODM98) and the same 325 nm CW laser source as used in the PL measurements. Signals were sent to a LN cooled CCD/spectrometer (PI Acton) via an optical fiber. Samples were placed on a holder in the center of the integrating sphere at a slight angle. The intensity of the 325 nm source was measured in both a hit and miss configuration to calculate the absorption percent.

A home-built confocal fluorescence microscope was used to measure PL decay times of InGaN nanowire arrays. The 267 nm excitation source was derived from the third harmonic of the 800 nm output from a Ti:sapphire regenerative amplifier (Coherent RegA9000), which produces ∼200 fs pulses at a 295 kHz repetition rate. A small portion of the excitation source was picked off and measured on a fast photodiode. The remainder was attenuated to powers ranging from 0.4 to 30 $\mu$W using neutral density filters and focused on the nanowire sample to a diameter of 750 nm using an objective with NA = 0.8. The PL was back-collected through the same objective and focused onto a single photon counting avalanche photodiode (APD, PDM series, MPD). The band-edge emission from InGaN nanowires was isolated by using a set of visible wavelength filters. The fast photodiode and APD signals were read into a time-correlated single photon counting (TCSPC) card (PicoHarp300, PicoQuant). The timing card collected photon arrival times in 4 ps bins, although the time resolution of the measurement is limited by the detector response time. Instrument response functions (IRF) were measured to have a FWHM of 48 ps.


dx.doi.org/10.1021/jp311685x | J. Phys. Chem. C XXXX, XXX, XXX−XXX

## ■ ASSOCIATED CONTENT

### Supporting Information

HAADF STEM images, XRD spectra, PL spectra, color PL images, time-resolved PL spectra of as grown, and annealed $In_xGa_{1-x}N$ nanowires. This material is available free of charge via the Internet at http://pubs.acs.org.

## ■ AUTHOR INFORMATION


### Corresponding Author

*E-mail p_yang@berkeley.edu.


### Notes

The authors declare no competing financial interest.

## ■ ACKNOWLEDGMENTS

This work was supported by the Director, Office of Science, Office of Basic Energy Sciences, Materials Sciences and Engineering Division, of the U.S. Department of Energy under Contract DE-AC02-05CH11231. We thank the National Center for Electron Microscopy for the use of their facilities. Special thanks to Shaul Aloni, Tev Kuykendall, Yun Jeong Hwang, and Cheng Hao Wu for scientific discussions.

## ■ REFERENCES


(1) Wu, J. Q. When Group-III Nitrides Go Infrared: New Properties and Perspectives. *J. Appl. Phys.* **2009**, *106*, 011101.

(2) Phillips, J. M.; Coltrin, M. E.; Crawford, M. H.; Fischer, A. J.; Krames, M. R.; Mueller-Mach, R.; Mueller, G. O.; Ohno, Y.; Rohwer, L. E. S.; Simmons, J. A.; et al. Research Challenges to Ultra-Efficient Inorganic Solid-State Lighting. *Laser Photon. Rev.* **2007**, *1*, 307−333.

(3) Hwang, Y. J.; Wu, C. H.; Hahn, C.; Jeong, H. E.; Yang, P. D. Si/InGaN Core/Shell Hierarchical Nanowire Arrays and Their Photoelectrochemical Properties. *Nano Lett.* **2012**, *12*, 1678−1682.

(4) Wu, J.; Walukiewicz, W.; Yu, K. M.; Shan, W.; Ager, J. W.; Haller, E. E.; Lu, H.; Schaff, W. J.; Metzger, W. K.; Kurtz, S. Superior Radiation Resistance of $In_{1-x}Ga_xN$ Alloys: Full-Solar-Spectrum Photovoltaic Material System. *J. Appl. Phys.* **2003**, *94*, 6477−6482.

(5) Moses, P. G.; Miao, M. S.; Yan, Q. M.; Van de Walle, C. G. Hybrid Functional Investigations of Band Gaps and Band Alignments for AlN, GaN, InN, and InGaN. *J. Chem. Phys.* **2011**, *134*, 084703.

(6) Khan, A. Semiconductor Photonics: Laser Diodes Go Green. *Nat. Photonics* **2009**, *3*, 432−434.

(7) Stringfellow, G. B. Microstructures Produced During the Epitaxial Growth of InGaN Alloys. *J. Cryst. Growth* **2010**, *312*, 735−749.

(8) Guo, W.; Zhang, M.; Banerjee, A.; Bhattacharya, P. Catalyst-Free InGaN/GaN Nanowire Light Emitting Diodes Grown on (001) Silicon by Molecular Beam Epitaxy. *Nano Lett.* **2010**, *10*, 3355−3359.

(9) Kuykendall, T.; Ulrich, P.; Aloni, S.; Yang, P. Complete Composition Tunability of InGaN Nanowires Using a Combinatorial Approach. *Nat. Mater.* **2007**, *6*, 951−956.

(10) Hahn, C.; Zhang, Z. Y.; Fu, A.; Wu, C. H.; Hwang, Y. J.; Gargas, D. J.; Yang, P. D. Epitaxial Growth of InGaN Nanowire Arrays for Light Emitting Diodes. *ACS Nano* **2011**, *5*, 3970−3976.

(11) Xiang, H. J.; Wei, S. H.; Da Silva, J. L. F.; Li, J. B. Strain Relaxation and Band-Gap Tunability in Ternary $In_xGa_{1-x}N$ Nanowires. *Phys. Rev. B* **2008**, *78*, 193301.

(12) Chuo, C. C.; Lee, C. M.; Chyi, J. I. Interdiffusion of In and Ga in InGaN/GaN Multiple Quantum Wells. *Appl. Phys. Lett.* **2001**, *78*, 314−316.

(13) Lin, Y. S.; Ma, K. J.; Chung, Y. Y.; Feng, S. W.; Cheng, Y. C.; Lin, E. C.; Yang, C. C.; Kuo, C. T.; Tsang, J. S. A Microstructure Study of Post-Growth Thermally Annealed InGaN/GaN Quantum Well Structures of Various Well Widths. *J. Cryst. Growth* **2003**, *252*, 107−112.

(14) Shin, H.; Arkun, E.; Thomson, D. B.; Miraglia, P.; Preble, E.; Schlesser, R.; Wolter, S.; Sitar, Z.; Davis, R. F. Growth and Decomposition of Bulk GaN: Role of the Ammonia/Nitrogen Ratio. *J. Cryst. Growth* **2002**, *236*, 529−537.

(15) Northrup, J. E.; Romano, L. T.; Neugebauer, J. Surface Energetics, Pit Formation, and Chemical Ordering in InGaN Alloys. *Appl. Phys. Lett.* **1999**, *74*, 2319−2321.

(16) Stampfl, C.; Van de Walle, C. G. Energetics and Electronic Structure of Stacking Faults in AlN, GaN, and InN. *Phys. Rev. B* **1998**, *57*, 15052−15055.

(17) Zywietz, T.; Neugebauer, J.; Scheffler, M. Adatom Diffusion at GaN (0001) and (000(1)over-Bar) Surfaces. *Appl. Phys. Lett.* **1998**, *73*, 487−489.

(18) Potin, V.; Ruterana, P.; Nouet, G.; Pond, R. C.; Morkoc, H. Mosaic Growth of GaN on (0001) Sapphire: A High-Resolution Electron Microscopy and Crystallographic Study of Threading Dislocations from Low-Angle to High-Angle Grain Boundaries. *Phys. Rev. B* **2000**, *61*, 5587−5599.

(19) Jenichen, B.; Brandt, O.; Pfuller, C.; Dogan, P.; Knelangen, M.; Trampert, A. Macro- and Micro-Strain in GaN Nanowires on Si(111). *Nanotechnology* **2011**, *22*, 295714.

(20) Gargas, D. J.; Gao, H. W.; Wang, H. T.; Yang, P. D. High Quantum Efficiency of Band-Edge Emission from ZnO Nanowires. *Nano Lett.* **2011**, *11*, 3792−3796.

(21) Tonti, D.; van Mourik, F.; Chergui, M. On the Excitation Wavelength Dependence of the Luminescence Yield of Colloidal CdSe Quantum Dots. *Nano Lett.* **2004**, *4*, 2483−2487.

(22) Krestnikov, I. L.; Ledentsov, N. N.; Hoffmann, A.; Bimberg, D.; Sakharov, A. V.; Lundin, W. V.; Tsatsul'nikov, A. F.; Usikov, A. S.; Alferov, Z. I.; Musikhin, Y. G.; et al. Quantum Dot Origin of Luminescence in InGaN-GaN Structures. *Phys. Rev. B* **2002**, *66*, 155310.

(23) Pophristic, M.; Long, F. H.; Tran, C.; Ferguson, I. T.; Karlicek, R. F. Time-Resolved Photoluminescence Measurements of InGaN Light-Emitting Diodes. *Appl. Phys. Lett.* **1998**, *73*, 3550−3552.

(24) Berberan-Santos, M. N.; Bodunov, E. N.; Valeur, B. Mathematical Functions for the Analysis of Luminescence Decays with Underlying Distributions. 1. Kohlrausch Decay Function (Stretched Exponential). *Chem. Phys.* **2005**, *315*, 171−182.

(25) Lindsey, C. P.; Patterson, G. D. Detailed Comparison of the Williams-Watts and Cole-Davidson Functions. *J. Chem. Phys.* **1980**, *73*, 3348−3357.

(26) Singh, J.; Bajaj, K. K. Theory of Excitonic Photoluminescence Linewidth in Semiconductor Alloys. *Appl. Phys. Lett.* **1984**, *44*, 1075−1077.

(27) Khatsevich, S.; Rich, D. H.; Zhang, X.; Dapkus, P. D. Correlating Exciton Localization with Compositional Fluctuations in InGaN/GaN Quantum Wells Grown on GaN Planar Surfaces and Facets of GaN Triangular Prisms. *J. Appl. Phys.* **2007**, *102*, 093502.

(28) Shockley, W.; Queisser, H. J. Detailed Balance Limit of Efficiency of P-N Junction Solar Cells. *J. Appl. Phys.* **1961**, *32*, 510.

(29) Liu, W.; Tan, R. J. N.; Soh, C. B.; Chua, S. J. The Effects of Cap Layers on Electrical Properties of Indium Nitride Films. *Appl. Phys. Lett.* **2010**, *97*, 042110.

(30) Chevtchenko, S. A.; Reshchikov, M. A.; Fan, Q.; Ni, X.; Moon, Y. T.; Baski, A. A.; Morkoc, H. Study of $SiN_x$ and $SiO_2$ Passivation of GaN Surfaces. *J. Appl. Phys.* **2007**, *101*, 113709.

(31) Martinez, G. L.; Curiel, M. R.; Skromme, B. J.; Molnar, R. J. Surface Recombination and Sulfide Passivation of GaN. *J. Electron. Mater.* **2000**, *29*, 325−331.

(32) Albrecht, M.; Neugebauer, J.; Ruterana, P. *Nitride Semiconductors: Handbook on Materials and Devices*; Wiley-VCH: Weinheim, 2003.